Energy & Environmental Science

PAPER

View Article Online
View Journal

Cite this: DOI: 10.1039/c9ee02020a

The impact of energy alignment and interfacial recombination on the internal and external open-circuit voltage of perovskite solar cells†

Martin Stolterfoht, *[a] Pietro Caprioglio, [ab] Christian M. Wolff, [a] José A. Márquez,[c] Joleik Nordmann,[a] Shanshan Zhang,[a] Daniel Rothhardt,[a] Ulrich Hörmann,[a] Yohai Amir,[a] Alex Redinger, [h] Lukas Kegelmann, [b] Fengshuo Zu,[de] Steve Albrecht,[b] Norbert Koch, [de] Thomas Kirchartz, [f] Michael Saliba, [g] Thomas Unold*[c] and Dieter Neher *[a]

Received 6th May 2019,
Accepted 3rd July 2019

DOI: 10.1039/c9ee02020a

rsc.li/ees

Charge transport layers (CTLs) are key components of diffusion controlled perovskite solar cells, however, they can induce additional non-radiative recombination pathways which limit the open circuit voltage (V_{OC}) of the cell. In order to realize the full thermodynamic potential of the perovskite absorber, both the electron and hole transport layer (ETL/HTL) need to be as selective as possible. By measuring the photoluminescence yield of perovskite/CTL heterojunctions, we quantify the non-radiative interfacial recombination currents in *pin*- and *nip*-type cells including high efficiency devices (21.4%). Our study comprises a wide range of commonly used CTLs, including various hole-transporting polymers, spiro-OMeTAD, metal oxides and fullerenes. We find that all studied CTLs limit the V_{OC} by inducing an additional non-radiative recombination current that is in most cases substantially larger than the loss in the neat perovskite and that the least-selective interface sets the upper limit for the V_{OC} of the device. Importantly, the V_{OC} equals the internal quasi-Fermi level splitting (QFLS) in the absorber layer only in high efficiency cells, while in poor performing devices, the V_{OC} is substantially lower than the QFLS. Using ultraviolet photoelectron spectroscopy and differential charging capacitance experiments we show that this is due to an energy level mis-alignment at the *p*-interface. The findings are corroborated by rigorous device simulations which outline important considerations to maximize the V_{OC}. This work highlights that the challenge to suppress non-radiative recombination losses in perovskite cells on their way to the radiative limit lies in proper energy level alignment and in suppression of defect recombination at the interfaces.

Broader context

As perovskite solar cells continue to improve at a rapid pace, more fundamental insights into the remaining open-circuit voltage (V_{OC}) losses are required in order to unlock power conversion efficiencies (PCEs) of ~30%. Several studies highlight that the perovskite absorber exhibits an opto-electronic quality that is comparable to GaAs in terms of external fluorescence, therefore potentially allowing PCEs close to the radiative limits. However, the high internal potential in the absorber layer can often not be directly translated into an equal potential at the metal electrodes. In this work, we reveal the reasons for the discrepancy by decoupling the main V_{OC} losses in the bulk, perovskite/charge transport layer (CTL) interfaces and/or metal contacts for a broad range of different perovskite compositions and several, commonly used CTLs. Undoubtedly, by introducing additional non-radiative recombination centres at the interfaces, the CTLs have the most striking impact on the device V_{OC}. Moreover, interface recombination is often exponentially increased in case of an energy level mismatch between the perovskite and the CTLs. We conclude that energy level matching is of primary importance to achieve the implied V_{OC} of the perovskite/CTL stack, followed by suppression of defect recombination at the interfaces and in the absorber layer.

[a] Institute of Physics and Astronomy, University of Potsdam, Karl-Liebknecht-Str. 24-25, D-14476 Potsdam-Golm, Germany. E-mail: stolterf@uni-potsdam.de, neher@uni-potsdam.de
[b] Young Investigator Group Perovskite Tandem Solar Cells, Helmholtz-Zentrum Berlin für Materialien und Energie GmbH, Kekuléstraße 5, 12489 Berlin, Germany
[c] Department of Structure and Dynamics of Energy Materials, Helmholtz-Zentrum-Berlin, Hahn-Meitner-Platz 1, D-14109 Berlin, Germany. E-mail: unold@helmholtz-berlin.de
[d] Helmholtz-Zentrum Berlin für Materialien und Energie GmbH, 12489 Berlin, Germany
[e] Institut für Physik & IRIS Adlershof, Humboldt-Universitat zu Berlin, 12489 Berlin, Germany
[f] Institut für Energie- und Klimaforschung, Forschungszentrum Jülich GmbH, 52425 Jülich, Germany
[g] Institute of Materials Science, Technical University of Darmstadt, Alarich-Weiss-Strasse 2, D-64287 Darmstadt, Germany
[h] Faculty of Science, Technology and Communication, Université du Luxembourg, L-1511 Luxembourg

† Electronic supplementary information (ESI) available. See DOI: 10.1039/c9ee02020a

Introduction

Huge endeavours are devoted to understanding and improving the performance of perovskite solar cells, which continue to develop at a rapid pace already outperforming other conventional thin-film technologies on small cells (<1 cm^2).[1] It is well established that further improvements will require suppression of non-radiative recombination losses to reach the full thermodynamic potential in terms of open-circuit voltage (V_{OC}) and fill factor (FF).[2] As such, a major focus of the entire field to push the technology forward is targeted at reducing defect recombination in the perovskite bulk with numerous works highlighting the importance of grain boundaries in determining the efficiency losses.[3,4] In contrast, many other studies highlight the significance of traps at the perovskite surface which is likely chemically distinct from the bulk.[4–6] In many cases, performance improvements were achieved by mixing additives into the precursor solution including multiple cations and/or halides.[6–9] In several studies, a slower transient photoluminescence (TRPL) decay is shown as the figure of merit to prove the suppressed trap-assisted recombination in the bulk while implying its positive impact on the overall device efficiency.[3,6,10] Significantly fewer publications have focused on the importance of non-radiative recombination of charges across the perovskite/CTL interface.[11–13] Until recently it has been challenging to pinpoint the origin of these free energy losses in complete cells, although there have been some studies with valuable insight.[11–15] Methods that have been employed to study interfacial recombination in perovskite stacks include impedance spectroscopy,[11,16] transient photoluminescence (TRPL)[13,17,18] or reflection spectroscopy (TRS),[14] transient microwave conductivity (TRMC),[15] and transient photovoltage (TPV).[19] Whilst these techniques exhibit in principle the required time resolution to unveil the kinetics of the interface and bulk recombination, the interpretation of these transient measurements can be very challenging. The reasons are related to the inherent fact that extraction and recombination can both reduce the emitting species in the bulk, thus causing the signal decay.[2] Previously, a more direct approach to decouple the origin of these recombination losses at each individual interface has been introduced based on steady-state photoluminescence measurements.[9,20–25] In particular, measurements of the emitted photoluminescence quantum yield (PLQY) on individual perovskite/transport layer junctions have been used to explain the V_{OC} through QFLS losses in the perovskite bulk and at the individual interfaces.[9,20,21] However, the relation between the internal QFLS and the external V_{OC} remains poorly understood today, especially for different solar cells architectures with different perovskite absorbers and/or charge transport layers. For example, in a recent study, a very high external PLQY (15%) has been reported on a *nip* stack (*i.e.* an electron transport layer/perovskite/hole transport layer junction) upon grain boundary passivation using potassium iodide.[9] Considering the provided external quantum efficiency (EQE), this high PLQY translates in an internal QFLS of $\sim$1.26 eV, which is very close to the radiative limit of the given perovskite absorber layer ($\sim$1.31 eV). Yet, the V_{OC} of the optimized cells was considerably lower (1.17 V). This suggests that interfacial recombination (which impacts the QFLS of the *nip* stack) is not causing the primary V_{OC} limitation and suggests that losses of $\sim$100 mV are of different nature. This raises the important question whether the external V_{OC} as measured on a complete solar cell truly represents the QFLS in the perovskite bulk and how this depends on the strength of interfacial defect recombination or the energy level alignment between the perovskite and the transport layers. Until today, the importance and impact of energy level alignment remains an important, yet heavily debated topic in perovskite solar cells. For example, several studies showed the benefit or a large impact of energy level alignment between the perovskite and the transport layers,[13,26–28] which was however challenged in other works.[29]

In this work, we studied the relation between the QFLS and the V_{OC} by means of absolute PL measurements in ''regular'' (*nip*-type)[7,30,31] and ''inverted'' (*pin*-type)[32–34] perovskite solar cells for a broad range of CTLs including metal oxides, conjugated polymers,[6,35] small molecules, and fullerenes. First, we aimed to compare the selectivity of CTLs used for *nip* and *pin* configurations in triple cation perovskite cells; *i.e.* for instance TiO_2 or SnO_2 *vs.* PTAA underneath the perovskite or doped spiro-OMeTAD *vs.* C_{60} on top. We note that in this work we define the selectivity of a CTL as its ability to maintain the QFLS of the absorber layer while providing efficient majority carrier extraction. The results suggest that when attached to the perovskite, all studied CTL cause a reduction of the QFLS with respect to the QFLS of the neat perovskite on a fused silica substrate (1.23 eV). The results were also generalized to different perovskite absorber layers. A comparison of the QFLS obtained on CTL/perovskite (or perovskite/CTL) bilayers and *nip*- or *pin* stacks, suggests a simple superposition principle of non-radiative recombination currents at each individual interface. This implies that the inferior interface dominates the free energy loss in the complete cell. In efficient cells, where the QFLS matches the device V_{OC}, we can further estimate the parallel recombination currents in the bulk, interfaces and/or metal contacts under V_{OC} conditions. However, in poor performing cells we find that the V_{OC} is substantially lower than the corresponding QFLS of the *pin* stack. Drift diffusion simulations highlight the impact of energy level offsets in causing the mismatch between the internal QFLS and the external V_{OC} which we further confirmed using photoemission spectroscopy (UPS) and transient differential charging capacitance experiments. The results underline that the primary non-radiative recombination loss channel of today's perovskite cells is interfacial recombination at (or across) the perovskite/CTL interface and that interfacial recombination is often exponentially increased in case of an energy level offset between the perovskite and the TLs. As such, our findings highlight the importance of tailoring the energetics and kinetics at the perovskite/CTL interfaces to harvest the full potential in perovskite solar cells.

Materials

The studied CTLs in this work belong to 3 material classes, conjugated polymers, small molecules and metal oxides.

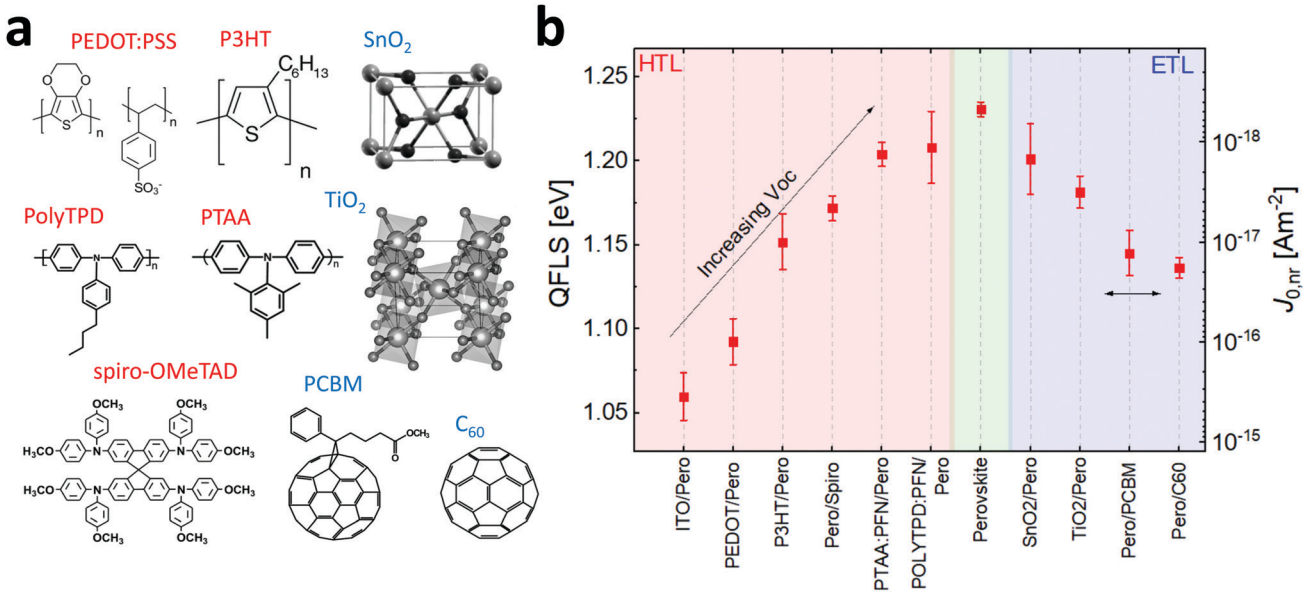

Fig. 1 The optoelectronic quality of triple cation perovskite/CTL layer junctions. (a) Materials studied in this paper. (b) The quasi-Fermi level splitting of the studied heterojunctions with different hole and electron transporting materials and of the neat absorber layer calculated based on eqn (2) using absolute photoluminescence measurements. The absorber was spin casted from the same solution for all transport layers. The non-radiative dark saturation current is plotted on the right and was obtained from $J_{0,nr} = J_0 - J_{0,rad}$ which allows comparing the strength of non-radiative recombination of different junctions.

Regarding the conjugated polymers, we studied highly selective wide-band gap donors such as PolyTPD and PTAA.[6,35] Poly({9,9-bis[30-({*N*,*N*-dimethyl}-*N*-ethylammonium)-propyl]-2,7-fluorene}-*alt*-2,7-{9,9-di-*n*-octylfluorene}) dibromide (here "PFN") was added on top of both materials to improve the wettability. In order to draw correlations between the QFLS and the energetics of the HTL, we also investigated P3HT,[36,37] as well as the highly conductive composite PEDOT:PSS.[12] As small molecule HTL, we tested spiro-OMeTAD[38,39] which requires doping by different ionic salts and other additives.[39] For the case of small molecule ETLs, we tested the fullerene C_{60} (with and without the interlayer LiF[20]) and the solution-processable fullerene derivative PCBM.[34,40] Lastly, we studied the commonly used transparent metal oxides TiO_2 and SnO_2. TiO_2 is widely considered as an ideal electron transporting layer due to its high selectivity and high charge carrier mobility,[41] while SnO_2 is the preferred platform for planar efficient *nip* cells.[11] These chemical structures of the materials are shown in Fig. 1. As absorber layer we chose the so-called triple cation perovskite $(CsPbI_3)_{0.05}[(FAPbI_3)_{0.83}(MAPbBr_3)_{0.17}]_{0.95}$ (see ESI,† Methods),[8] while the study was later extended to other perovskite systems as discussed below.

Comparison of CTLs for *pin* and *nip* type devices

In order to quantify the free energy losses at the CTL/perovskite interface, we measured the absolute photoluminescence (PL) yield of perovskite/transport layer heterojunctions. The absolute PL is a direct measure of the quasi-Fermi level splitting (QFLS or μ) in the absorber,[24,42–45] and this approach has been recently applied to perovskite solar cells by various groups.[20–23] The ratio of emitted (ϕ_{em}) and absorbed photon fluxes (ϕ_{abs}) defines the absolute external PL quantum yield (PLQY):

$$\mathrm{PLQY} = \frac{\phi_{em}}{\phi_{abs}} = \frac{J_{rad}/e}{J_G/e} = \frac{J_{rad}}{J_{R,tot}} = \frac{J_{rad}}{J_{rad} + J_{non\text{-}rad}} = \frac{J_{rad}}{J_{rad} + J_B + J_{p\text{-}i} + J_{i\text{-}n} + \ldots} \quad (1)$$

If all emission is from the direct recombination of free charges, and also every absorbed photon generates a free electron–hole pair, the PLQY equals the ratio of the radiative recombination current density (J_{rad})[42] and the total free charge generation current density (J_G). At V_{OC}, charge extraction is zero, meaning that J_G is equal to the total recombination current ($J_{R,tot}$) of radiative and non-radiative losses ($J_{rad} + J_{non\text{-}rad}$). Furthermore, $J_{non\text{-}rad}$ is equal to the sum of all non-radiative recombination pathways in the bulk (J_B), at the HTL/perovskite ($J_{p\text{-}i}$) and the perovskite/ETL ($J_{i\text{-}n}$) interface, and potentially other losses (*e.g.* recombination in the transport layers, or at the CTL/metal interfaces). Using the expression for the radiative recombination current density according to Shockley–Queisser[42] and eqn (1), we can write the QFLS (μ) as a function of the radiative efficiency

$$J_{rad} = J_{0,rad} e^{\mu/kT} \rightarrow \mu = kT \ln\left(\frac{J_{rad}}{J_{0,rad}}\right) = kT \ln\left(\mathrm{PLQY}\frac{J_G}{J_{0,rad}}\right) = kT \ln\left(\frac{J_G}{J_0}\right) = kT \ln\left(\frac{J_{rad}}{J_{rad} + J_B + J_{p\text{-}i} + J_{i\text{-}n} + \ldots}\frac{J_G}{J_{0,rad}}\right) \quad (2)$$

where $J_{0,rad}$ is the radiative thermal equilibrium recombination current density in the dark and $J_0 = J_{0,rad}/\mathrm{PLQY}$ the dark saturation current. We note, that the PLQY depends itself on external conditions such as the illumination intensity or the

Table 1 Optoelectronic quality of several tested perovskite–CTL layer junctions

Film	Absorption	PLQY	$J_{0,nr}$ [A m^{-2}]	QFLS [eV]
ITO/Pero	0.839	2.0×10^{-5}	3.5×10^{-16}	1.060
PEDOT:PSS/Pero	0.854	7.5×10^{-5}	9.9×10^{-17}	1.092
P3HT/Pero	0.848	7.7×10^{-4}	1.0×10^{-17}	1.152
Pero/spiro-OMeTAD	0.944	1.4×10^{-3}	4.6×10^{-18}	1.172
PTAA/PFN/Pero	0.852	5.1×10^{-3}	1.3×10^{-18}	1.204
PolyTPD/PFN/Pero	0.851	7.3×10^{-3}	1.1×10^{-18}	1.208
Pero	0.850	1.4×10^{-2}	4.6×10^{-19}	1.231
SnO_2/Pero	0.854	5.9×10^{-3}	1.5×10^{-18}	1.201
TiO_2/Pero	0.854	2.1×10^{-3}	3.2×10^{-18}	1.181
Pero/PCBM	0.934	5.7×10^{-4}	1.3×10^{-17}	1.145
Pero/C_{60}	0.927	3.8×10^{-4}	1.8×10^{-17}	1.137
Pero/LiF/C_{60}	0.892	1.3×10^{-3}	4.9×10^{-18}	1.170

internal QFLS. This originates from the fact that the non-radiative recombination pathways depend differently on the actual number of charge pairs present in the device compared to radiative recombination.[46] Thus, in order to predict the QFLS under 1 sun and open-circuit, the PLQY needs to be measured under the same illumination conditions. Eqn (2) also shows that the QFLS depends logarithmically on the non-radiative recombination currents in the bulk, interface *etc.* In order to quantify the QFLS, the generated current density under illumination (J_G) and $J_{0,rad}$ need to be known, as well as the thermal energy (we measured a temperature of ~26–28 °C on the sample under 1 sun equivalent illumination using a digital standard infrared sensor). J_G and $J_{0,rad}$ are obtained from the integrated product of the external quantum efficiency (EQE) and the solar photon flux (ϕ_{sun}) at 300 K and the black body spectrum (ϕ_{BB}), respectively.[42,43,47,48] As such, we obtained a $J_{0,rad}$ of $\sim 6.5 \times 10^{-21}$ A m^{-2} ($\pm 1 \times 10^{-21}$ A m^{-2}) independent of the bottom CTL (ESI,† Fig. S1) as it is predominantly determined by the tail absorption of the triple cation perovskite absorber layer (with Urbach energies around 15 meV). In all cases, the QFLS was measured by illuminating the films through the perovskite (or the transparent layer in case of *pin* or *nip* stacks) in order to avoid parasitic absorption of the studied CTL (see ESI,† Fig. S2). The results of the PL measurements of the different transport layers are summarized in Table 1 and plotted in Fig. 1b. All results were obtained as an average of multiple fabricated films (ESI,† Fig. S3) with representative PL spectra shown in ESI,† Fig. S4. Details of the measurements conditions are discussed in ESI,† Methods.

Fig. 1b shows that the triple cation perovskite on a fused silica substrate limits the QFLS to approximately 1.231 eV, which is ~110 meV below the radiative V_{OC} limit (where the PLQY equals 1). We note that we cannot rule out that this value is limited by recombination at the fused silica/perovskite interface and also that we observe a substantially lower QFLS (~40 meV) of the bare perovskite layer on a glass substrate (see ESI,† Fig. S5). Moreover, significantly higher PLQY values above 20% were observed on methylammonium lead triiodide films where the top surface was passivated with tri-*n*-octylphosphine oxide (TOPO).[49] These results highlight the high opto-electronic quality of the perovskite bulk comparable (or already better) than highly pure silicon or GaAs but also indicates substantial recombination losses at the perovskite top surface. For the HTL/perovskite junctions we also tested the influence of the underlying ITO layer, however this did not significantly influence the obtained QFLS within a small error except for samples with SnO_2 (see ESI,† Fig. S3). Likewise, we tested the influence of the copper metal electrode on top of the C_{60} in perovskite/C_{60} heterojunctions and *pin* stacks (ESI,† Fig. S6). Overall, these tests suggest that there is usually a lossless charge transfer between the CTLs and the metal electrodes. Interestingly, Fig. 1b shows that the polymers PTAA/PFN and PolyTPD/PFN performed best – even outperforming the omnipresent spiro-OMeTAD. However, it is clear that the selectivity of a TL can be different underneath or on top of the perovskite. Therefore, we do not aim to quantify the opto-electronic quality of a CTL itself but rather assess the selectivity of the CTL in a particular configuration (*i.e.* either on top or underneath a particular perovskite layer). Among the studied ETLs, SnO_2 and TiO_2 outperform the organic ETLs C_{60} and PCBM which are usually used in *pin*-type cells. Therefore, this data suggests that the *p*-interface is the limiting interface for *nip* cells, and the *n*-interface for *pin* cells consistent with earlier studies.[21] Moreover, we observe that the capping CTLs PCBM and C_{60} are worse than spiro-OMeTAD. Considering that the inferior interface will dominate the final V_{OC} (eqn (1) and (2)), this might be one reason for the superior performance of *nip* cells today. One approach to suppress non-radiative recombination at the perovskite/C_{60} interface in *pin* cells is to insert a thin LiF interlayer as demonstrated earlier[20] and in Table 1.

A frequently arising question is how much the perovskite morphology, which potentially varies depending on the underlying CTL, could influence the obtained QFLS and the interpretation of the results. Thus, we performed top scanning electron microscopy and AFM measurements (see ESI,† Fig. S7). Interestingly, we find the largest grains on a PEDOT:PSS bottom CTL despite it being the worst among the studied transport layers. The largest grain size distribution is visible on perovskite films on TiO_2 while the perovskite morphology on all other substrates appears, at least qualitatively, similar where we observe relatively small grains (<10–100 nm). In addition, AFM measurements reveal root mean square surface roughnesses varying from 12–27 nm, where the perovskite on PolyTPD/PFN and PTAA/PFN appears to be roughest (>20 nm) while the perovskite film on TiO_2 is the smoothest. We also note the similar Urbach tail of the perovskite absorber layer when processed on different CTLs (ESI,† Fig. S1) which is related to the density of subgap states. This further indicates a similar opto-electronic quality of the perovskite. Considering these results, it seems unlikely that the perovskite bulk morphology can explain the changes in the non-radiative recombination loss currents which increase by orders of magnitude depending on the underlying substrate (as shown in Fig. 1b). It is also worth to note that these results do not allow distinguishing whether the critical recombination loss occurs across the perovskite/CTL interface, or at the perovskite surface next to the interface. In any case, the presence of the additional CTL triggers additional

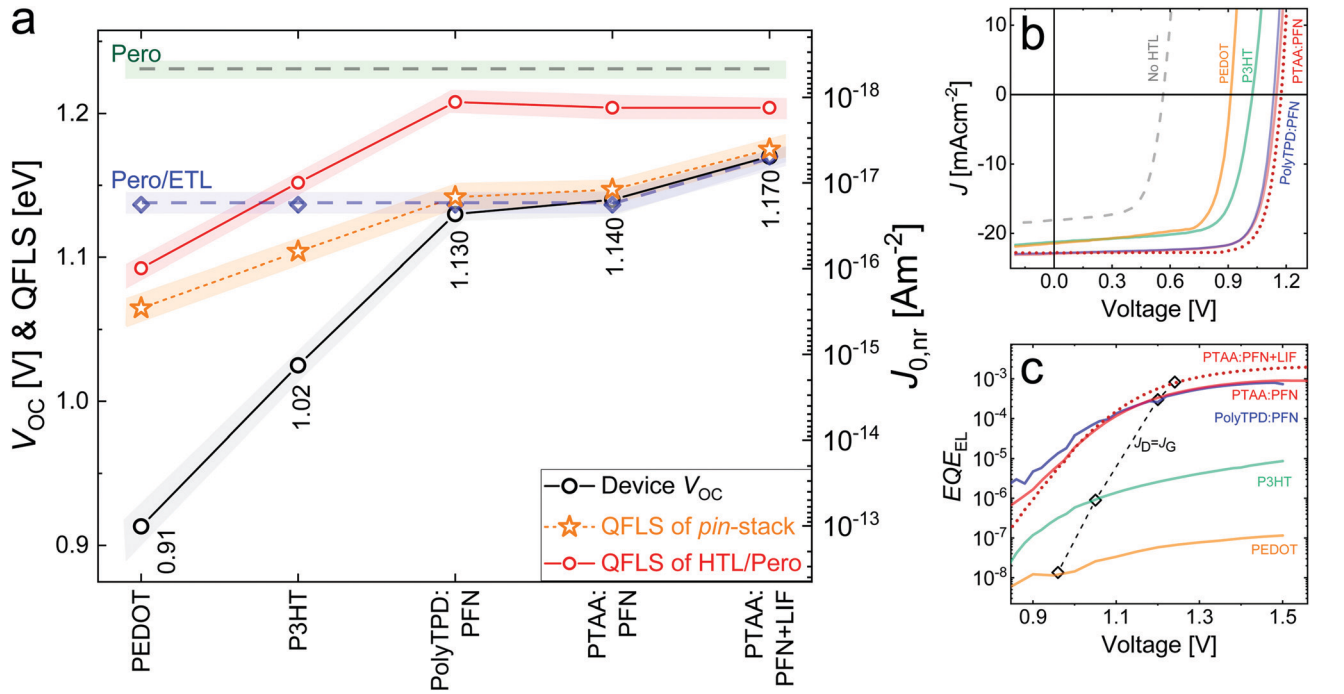

Fig. 2 Open-circuit voltage, quasi-Fermi level splitting and electroluminescence of *pin* cells. (a) Average V_{OC} of *pin* cells employing different conjugated polymers as HTLs and a C_{60} ETL, compared to the average QFLS of the corresponding HTL/perovskite bilayers (red), and of the *pin* stacks (orange). The QFLS of the perovskite/C_{60} junction and of the neat perovskite on fused silica are shown in dashed blue and green lines, respectively. The dark saturation current ($J_{0,nr} = J_0 - J_{0,rad}$) as plotted on the right allows to compare the strength of non-radiative recombination of different junctions. (b) Corresponding current density *vs.* voltage characteristics of the *pin* cells with different HTLs, and (c) the external electroluminescence efficiency as a function of voltage. The dashed line shows conditions where the dark injection and light generation currents are equal for each device.

(non-radiative) interfacial recombination losses, which are dominating the non-radiative recombination losses.

Comparison of the QFLS and device V_{OC} and origin of free energy losses

In the following, we aim to compare the non-radiative recombination losses at the *p*- and *n*-interfaces with the QLFS of the *pin* stacks and the V_{OC} of the complete cells with different HTLs and (LIF/)C_{60} as ETL. Fig. 2a shows that the device V_{OC} (black line) generally increases with the average QFLS of the *pin* stack (orange line) which was taken as an average as obtained on 3–4 samples for each configuration. Importantly, for optimized cells with PolyTPD or PTAA, the V_{OC} (black line) matches the QFLS of the stack (orange line) within a small error. This is also nearly identical to the QFLS of the less selective perovskite/C_{60} interface (blue line). This indicates that for these particular cells, the losses determining the V_{OC} occur almost entirely at the inferior interface to the perovskite while the electrodes are not causing additional V_{OC} losses. On the other hand, in case of the less selective PEDOT:PSS and P3HT bottom layers, the V_{OC} was found to be substantially lower than the corresponding QFLS. This will be discussed further below. The current density *vs.* voltage (*JV*) characteristics of the corresponding cells are shown in Fig. 2b which highlight the large differences in the measured V_{OC}s. Device statistics of individually measured stacks are shown in ESI,† Fig. S9. We note that our devices with LiF/C_{60} as ETL reach efficiencies of up to 21.4% with a V_{OC} of ~1.2 V (for a triple cation perovskite with a bandgap of ~1.6 eV), which is among the highest reported values for *pin*-type cells (ESI,† Fig. S10).[50–52]

Next, we compared the PLQY with the external electroluminescence quantum efficiency (EQE_{EL}) as shown in Fig. 2c. Under conditions where the dark injection current equals the generation current, the EQE_{EL} of PTAA and PolyTPD cells (3×10^{-4} for both devices) approaches the PLQY of the stack within a factor of two (5.9×10^{-4} for PTAA and 4.6×10^{-4} for PolyTPD). Improving the perovskite/ETL interface by inserting LiF increases both the QFLS of the *pin* stack and the V_{OC} to 1.17 V corresponding to a PLQY of $\sim 1.3 \times 10^{-3}$ and EQE_{EL} of $\sim 8.3 \times 10^{-4}$.[20] However, for devices with PEDOT:PSS, the EQE_{EL} ($\sim 1.4 \times 10^{-8}$) is orders of magnitude lower than the PLQY of the stack ($\sim 1 \times 10^{-5}$). We note that the measured EQE_{EL} matches roughly the expected EQE_{EL} according to Rau's reciprocity for a V_{OC} of 0.9 V as obtained from the *JV* scan (3.8×10^{-8}). Therefore, we conclude that the inferior interface (PEDOT:PSS/perovskite) limits the QFLS of the stack, however, there is an additional loss which affects the V_{OC} but not the QFLS. This will be addressed further below. Lastly, films with P3HT lie somewhat in between PEDOT:PSS and PTAA (PolyTPD) devices. Here, both interfaces (P3HT/perovskite and perovskite/C_{60}) appear to be equally limiting the QFLS of the stack which also lies below the QFLS of the individual heterojunctions (bilayers). Similar to PEDOT:PSS devices, we observe a considerable mismatch between PLQY of the optical *pin* stack (6.2×10^{-5}) and the EQE_{EL} ($\sim 9 \times 10^{-7}$).

We note that the measured EQE_{EL} is again very close to the EQE_{EL} that is expected for a P3HT device with a V_{OC} of ~1.0 V (~1.8×10^{-6}).

As for the *nip* cells with SnO_2 and TiO_2 as the ETL, and SpiroOMeTAD as the HTL, we observe a similar trend as in our optimized *pin*-type cells with PTAA or PolyTPD, that is a close match between the average device V_{OC} (~1.15 V) and the average internal QFLS (1.161 eV and 1.168 eV for TiO_2 and SnO_2 based cells, respectively) under 1 sun conditions. All results obtained on *nip* cells are shown in ESI,† Fig. S11. Regarding the potential impact of the perovskite morphology when the samples are prepared on different hole (electron) transport layers, it is important to note that the losses in the neat material (dashed green in Fig. 2a) cannot be larger than the cumulative losses observed in the CTL/perovskite bilayers (red). Moreover, the match between the QFLS of the glass/perovskite/CTL bilayers (blue) and the *pin* or *nip* stacks (Fig. 2a and ESI,† Fig. S11) means that the recombination at the top CTL interface can consistently explain the overall V_{OC} regardless, if the perovskite is deposited on glass or on the CTL (PTAA:PFN, PolyTPD:PFN, TiO_2, SnO_2). This highlights the importance of the top interface in determining the non-radiative recombination current in perovskite solar cells.

Quantification of parallel recombination currents at V_{OC}

The absolute-PL approach allows to further estimate the parallel recombination currents at V_{OC}. To this end, we successively quantify the non-radiative recombination currents in the neat material and the bottom and top interfaces from the PLQY of the corresponding perovskite/CTL films (eqn (1)) and knowledge of J_{rad} (eqn (2)). Important to note is that the PLQY of each film needs to be known at the V_{OC} or QFLS of the complete cell which requires intensity dependent PLQY measurements. Moreover, the individual recombination currents must add up to J_G which allows to the check the consistency of the approach. This is possible in efficient cells where the QFLS in the absorber layer matches the device eV_{OC} within a relatively small error (≈20 meV), but the procedure is prone to fail in cells where QFLS > eV_{OC}. Fig. 3a shows the obtained recombination currents for efficient *pin*-type and *nip*-type cells. Fig. 3b illustrates our optimized *pin* cells with LIF/C_{60} as ETL at V_{OC} by a bucket with holes which represent the recombination losses (see caption). We note again that the recombination current in the neat perovskite (turquoise) is obtained from a film on fused silica and therefore the loss in the neat absorber layer might be slightly different when deposited on top of a CTL. However, as we detail throughout the manuscript, changes in the perovskite morphology when deposited on different CTL cannot explain the V_{OC} of the final cells, and the fact that the recombination currents add up to J_G suggests that this loss estimation provides a realistic description of the parallel recombination currents at V_{OC}.

Understanding the QFLS across the *pin* (*nip*) junction

The experimental results in the previous sections show that QFLS ~ V_{OC} in case of good performing transport layers (PTAA and PolyTPD). This indicates that interfacial recombination in these devices lowers the QFLS throughout the whole bulk equally. However, in case of PEDOT:PSS or P3HT, the device V_{OC} is lower than the QFLS in the perovskite layer. In such cases, at least one QFL bends, presumably at the interfaces or contacts, causing a further reduction in the electrochemical potential of the photogenerated charges. This bending has a much larger effect on the final V_{OC} than on the average QFLS in the perovskite bulk. In order to check whether this

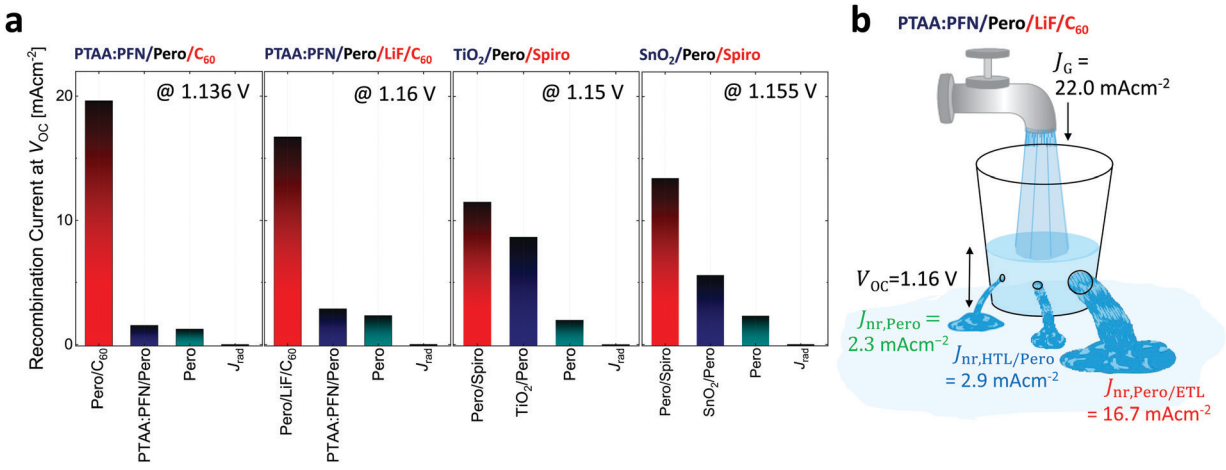

Fig. 3 (a) Bulk and interfacial non-radiative recombination currents at open-circuit as obtained on *nip* and *pin*-type cells with nearly flat quasi-Fermi levels. In *pin*-type cells, the non-radiative recombination current is dominated by the C_{60} interface (red) – even if optimized with LiF. In *nip*-type cells, the recombination at the upper perovskite/spiro-interface (red) dominates the recombination loss, although the recombination at the *p*- and *n*-interface are quite similar in case of cells based on TiO_2. In all cases, the non-radiative recombination losses in the neat perovskite (turquoise) are smaller than at the top interface. We note the radiative recombination current density is very small, *e.g.* 7.8 μA cm^{-2} in panel (a). (b) Illustrates a solar cell as bucket with holes where the water level represents the cells' V_{OC}.[53] The water stream from the tap corresponds to the generation current density from the sun. The holes in the bucket represent the recombination losses at V_{OC} in the bulk, interfaces *etc.* Depending on the exact size of the holes, the water level will change so as the V_{OC} of the device.

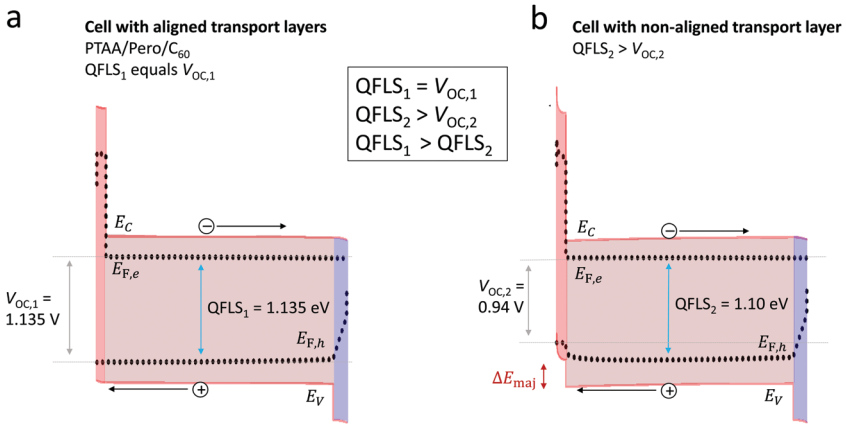

Fig. 4 Simulation of the QFLS and V_{OC} of *pin*-type devices using SCAPS. (a) The simulated quasi-Fermi level splitting (QFLS) in junctions with aligned transport layers (PTAA/perovskite/C_{60}) is identical to eV_{OC} but not in case of energetically mis-aligned transport layers (b) where the hole QFL bends at the interface to the hole transport layer which causes a QFLS–V_{OC} mismatch. The perovskite bandgap is represented in brown in between the conduction band minimum (E_C) and valence band maximum (E_V), while the dashed lines show the electron and hole quasi-Fermi levels ($E_{F,e}$ and $E_{F,h}$), the resulting QFLS in the absorber and the open-circuit voltage (V_{OC}) at the contacts. The HTL (red) and ETL (blue) are represented by their bandgaps in between the highest occupied and lowest unoccupied molecular orbitals.

phenomenon depends on the charge carrier generation profile, we analysed all samples by illuminating the samples through the bottom glass or top using a 445 nm laser (ESI,† Fig. S2) and through intensity and wavelength dependent V_{OC} measurements (ESI,† Fig. S12). However, we concluded that neither the QFLS nor the V_{OC} depend significantly on the charge generation profile, which we attribute to the rapid diffusion of charges through the perovskite. In order to understand the spatial distribution of the recombination losses and the QFLS, we simulated our perovskite solar cells using the well-established drift-diffusion simulator SCAPS.[54] These simulations take into account previously measured interface recombination velocities and perovskite bulk lifetimes.[20] The simulated electron/hole quasi-Fermi levels ($E_{F,e}$ and $E_{F,h}$) at open-circuit are shown along with the conduction and valence bands in Fig. 4a for a PTAA/PFN/perovskite/C_{60} device. Important simulation parameters listed in ESI,† Table S1. Qualitatively, these simulations confirm that $E_{F,e}$ and $E_{F,h}$ are spatially flat in the perovskite bulk and extend to the corresponding electrodes which explains that eV_{OC} is nearly identical to the QFLS (of ~1.13 eV) in these devices. Interestingly, to reproduce the comparatively high open-circuit voltages (~1.14 V) and FFs up to 80% of these devices, a considerable built-in voltage (V_{BI}) of at least 1.0 V had to be assumed considering realistic interface recombination velocities. Otherwise, a strong backfield would hinder charge extraction in forward bias but also accumulate minority carriers at the wrong contact (ESI,† Fig. S13). We note that the role of the V_{BI} across the absorber layer is currently an important topic in the community and further efforts need to be taken to properly consider the impact of ions on the field distribution.[55] Moreover, we had to assume a small majority carrier band offset ($\Delta E_{maj} < 0.1$ eV) between the perovskite valence/conduction band and the HOMO/LUMO of the HTL/ETL, respectively in order to reproduce the measured device V_{OC}.

Interestingly, the implementation of a majority carrier band offset at the *p*-interface causes a considerable bending of the hole quasi-Fermi level close to the interface which explains the QFLS–V_{OC} mismatch (Fig. 4b). Considering that $E_{F,e}$ and $E_{F,h}$ need to extend throughout the CTLs to the metal contacts in order to produce an external V_{OC}, it is clear that any ΔE_{maj} will cause an exponential increase of the hole population in the HTL. This implies an exponential increase in the recombination rate. Therefore, it is expected that a finite ΔE_{maj} will lead to an equal loss in the device V_{OC}. In order to generalize the conditions under which the V_{OC} deviates from the QFLS, we extended our simulations by studying a wide range of parameters (ESI,† Table S1). We found that at least two requirements must be fulfilled in order to explain the QFLS–V_{OC} mismatch: (a) a band offset for the majority carrier of at least ~0.2 eV, and (b) a sufficiently high recombination velocity (>1 cm s^{-1}), otherwise $E_{F,e}$ and $E_{F,h}$ can remain flat despite the energy offset (ESI,† Fig. S14). Indeed, these simulations show that the V_{OC} loss scales linearly with the ΔE_{maj} offset as long as the *p*-interface is limiting. We also note that the minority carrier band offset ΔE_{min} (*i.e.* the LUMO of the HTL and the perovskite conduction band) is not influencing the results if ΔE_{min} is larger than 0.1 eV which is further discussed at ESI,† Fig. S15. We also simulated a *pin* stack with a PEDOT:PSS bottom layer which we simplified by a metal with a work function of 5 eV, a high surface recombination velocity for holes and an intermediate value for electrons (ESI,† Table S1). For these settings we observed that $E_{F,h}$ bends up at the interface, giving rise to the experimentally observed QFLS–V_{OC} mismatch of roughly 150 meV in the PEDOT cell. All results on PEDOT:PSS cells are summarized in ESI,† Fig. S16. We acknowledge that these simulations only illustrate one possible scenario of the internal device energetics using a set of plausible parameters, and thus different energetic alignments or a morphological issue at the interface cannot be excluded. However, we can conclude that energy level alignment of all layers is a crucial requirement to

maximize the V_{OC} while the defect density at the interface is also a critical parameter in determining the non-radiative recombination losses.

Energy level alignment at the HTL/perovskite interface

The findings in the previous sections suggest that the observed mismatch between the internal QFLS and the V_{OC} in cells comprising PEDOT:PSS and P3HT is due to an energy offset at the *p*-interface. To study the energy level alignment between the perovskite and the transport layer, we first performed photoelectron yield spectroscopy measurements (PYS) on the individual layers of the solar cells (ESI,† Fig. S17). However, these measurements did not allow a reliable prediction of ΔE_{maj} which is due to the assumption of a constant vacuum level across different layers of the stack. To measure the energetic offsets between the perovskite and the transport layers with respect to the fixed Fermi level (E_F) of the ITO substrate, we performed UPS measurements with background illumination. Recently, it has been shown that the perovskite surface can be considerably n-doped,[56] which will directly impact the location of the valence band onset with respect to E_F when measuring the top surface of the perovskite film with a He beam (21.1 eV). However, when UPS is performed with an additional background light, the band bending at the surface can be flattened which then allows to access the bulk energy levels. This enabled a direct comparison between the energy levels of the transport layers and the perovskite bulk. Indeed, as shown in Fig. 5 below, by properly taking into account the surface photovoltage (SPV) effect, we found that the valence band of the perovskite is aligned with the HOMO of PTAA and PolyTPD HTLs, while P3HT and PEDOT:PSS exhibited states close to, or at the Fermi-edge. Thus, we conclude that PTAA and PolyTPD allow maintaining the high QFLS that is generated from the perovskite upon illumination which is in agreement with the drift diffusion simulations. In contrast, in case of P3HT, and even worse in case of PEDOT:PSS, carriers will lose part of their free energy once they are transferred from the perovskite to the HTL, thereby causing the additional V_{OC}-loss as numerically predicted and experimentally observed. A further confirmation of this picture comes from the measurement of the charge carrier density in the bulk (n_{bulk}) at a given V_{OC} using differential charging capacitance measurements.[57,58] In the case of proper energy alignment, n_{bulk} would be a sole function of the V_{OC}, independent of the choice of the TL material. The results in ESI,† Fig. S18 show that this is not the case. Instead, for a given V_{OC}, n_{bulk} is substantially larger for the PEDOT:PSS cell than for the P3HT and the PTAA cell with proper energy alignment. This is a direct consequence of the energy offset and the resulting difference between the QLFS and the device V_{OC} (see ESI,† Fig. S18d for a schematic representation of this situation).

Recombination losses in other perovskite systems

In order to generalize the findings, we also studied QFLS and V_{OC} losses in other currently popular perovskite materials (ESI,† Fig. S19). The results further confirm our main conclusions: (i) the perovskite bulk usually allows to reach higher V_{OC}s than ultimately achieved in the cell. This is confirmed in a low-gap triple

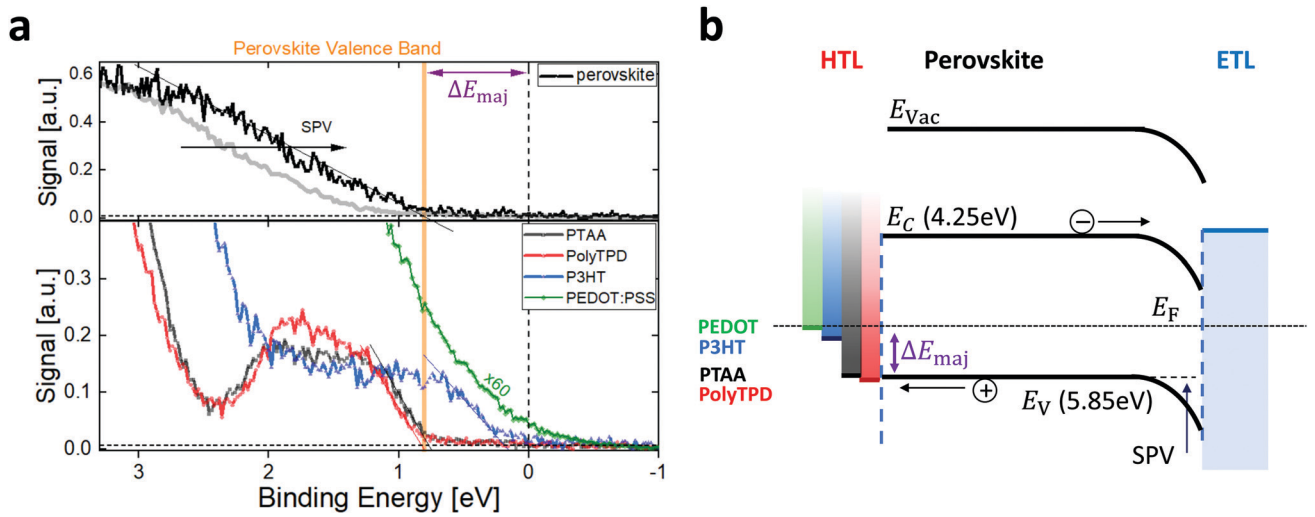

Fig. 5 (a) Ultraviolet photoelectron (UPS) spectra of PTAA, PolyTPD, P3HT and PEDOT:PSS on ITO. The corresponding signal of the perovskite film is shown above. The perovskite surface is n-doped[56] resulting in an apparent valence band onset of 1.35 eV. Application of a background light (with a 1 sun equivalent intensity) flattens the band bending at the surface which allows accessing the valence band onset in the perovskite bulk (0.8 eV away from the Fermi level).[56] The spectra of PEDOT:PSS is scaled by a factor of 60 as compared to the other films. As discussed by Hwang *et al.*,[59] a high-bandgap PSS layer is present on top of a solution processed film which weakens the photoelectron signal of states at the Fermi-edge of the underlying PEDOT:PSS bulk as shown in several publications.[59,60] The deduced energy levels are plotted in (b). As predicted from the QFLS–V_{OC} match in these cells, in case of PTAA and PolyTPD hole transport layers, the HOMO of the HTL is aligned with respect to the perovskite valence band. However, considerable majority carrier band offsets exist in case of P3HT and PEDOT:PSS. This causes the observed QFLS–V_{OC} mismatch as carriers relax to the band edges during their transport to the extracting electrode.

cation perovskite (~1.54 eV) which is currently used in the highest efficiency solar cells,[1] a hybrid vacuum/solution processed $MAPbI_3$ (~1.6 eV)[61] which is relevant for application on textured surfaces in tandem solar cells,[62] a high-gap mixed perovskite with a bandgap of 1.7 eV which is the ideal bandgap for monolithic Si/perovskite tandem solar cells, as well as two-dimensional perovskites based on *n*-butylammonium[63] – a popular system which demonstrates increased stability under thermal and environmental stress.[64] However, in some cases the QFLS of the optical stack is close to the QFLS of the neat absorber layer, *e.g.* for a solution processed $CsFAPbI_3$ (~1.47 eV) and $MAPbI_3$ (~1.6 eV). (ii) In most cases, the QFLS-PL technique can well describe the V_{OC} of the final cell which allows to assess the inferior interface by comparing the QFLS of HTL/perovskite or perovskite/ETL junctions. However, in a high-bandgap (~1.7 eV) mixed perovskite system we observe again a considerable mismatch between the QFLS of the *pin* stack and the V_{OC}. This suggests difficulties in increasing the perovskite bandgap while maintaining aligned energy levels and further demonstrates the relevance of our findings for other perovskite systems.

Conclusions

Using absolute PL measurements, we were able to decouple the origin of non-radiative recombination losses for cells in *pin* and *nip* configurations fabricated from different CTLs and perovskite compositions. For a triple cation perovskite system, we found that a range of commonly used CTLs induce large non-radiative recombination currents which dwarf the non-radiative losses in the neat perovskite. We identified that the most selective bottom CTLs are the polymers PTAA and PolyTPD and SnO_2 which are outperforming the omnipresent TiO_2 although this can vary depending on the exact preparation conditions and the absorber material. For *pin* cells the perovskite/C_{60} interface was found to be a major issue which induces more interfacial recombination than spiro-OMeTAD. This could be one reason for the lower performance of *pin*-type cells with the standard electron transporter C_{60}. A comparison between the QFLS of perovskite/CTL bilayers, optical *pin*- or *nip*-type stacks and the V_{OC} of the complete device shows that the relevant energy losses happen at the top interface in efficient triple cation cells based on PTAA and PolyTPD, SnO_2 and TiO_2. In these systems, the electron/hole QFLs are expected to be spatially flat throughout the junction to the electrodes, meaning that the QFLS in the perovskite bulk equals the V_{OC} of the cells. This allows further quantification of the parallel recombination currents in the bulk and interfaces and/or metal contacts which define the V_{OC} of the complete cell. However, in cells with energetically misaligned HTLs such as PEDOT or P3HT, the V_{OC} is lower than the QFLS in the absorber layer due to an internal bending of the hole-QFL. The fundamental study was validated in high-efficiency perovskite cells in *pin*-configuration with PCEs up to 21.4% and through rigorous device simulations. The simulations substantiated the understanding obtained from the experimental results and highlighted the importance of a high built-in voltage and negligible majority carrier band offsets between the perovskite and the transport layers. The presence of an energy level offset at the *p*-contact was confirmed with UPS and differential charging capacitance measurements. In order to generalize the findings, additional perovskite systems were studied which showed that the absorber layer often allows a substantially higher V_{OC} than achieved by the cell. However, a QFLS–V_{OC} mismatch in complete devices appears also in other systems than those featuring a triple cation absorber with PEDOT:PSS and P3HT HTLs. Therefore, this work allows to conclude that energetic offsets are often harming the device V_{OC} beyond the limitation imposed by defect recombination in the absorber layer and the interfaces. This implies that proper energy level alignment is a primary consideration to harvest the full potential of the optical *pin* or *nip* stack. Only then suppression of interfacial defect recombination will allow us to reach the potential of the perovskite absorber, while suppression of defects in the perovskite bulk or at grain boundaries and photon management will be the final goal to improve this technology to its radiative limit.

Author contributions

M. S. planned the project, drafted the manuscript, fabricated cells and films, performed electrical measurements, developed the PL setup, measured absolute PL and performed simulations and analysed all data. P. C. developed the PL setup, measured absolute PL. and data analysis, measured SEM and contributed to film fabrication and to manuscript drafting. C. M. W. provided important conceptual ideas regarding the identification of the recombination losses, cell fabrication and electrical characterization. J. A. M. performed PL measurements and performed corresponding data analysis and interpretation. J. N. performed PL measurements on cells and films and contributed to electrical measurements. S. Z. performed PESA and UV-Vis measurements and analysis of this data. D. R. fabricated cells and films, and contributed to electrical measurements. U. H. provided important conceptual ideas regarding the development of the PL setup and corresponding data analysis. Y. A. performed TPC, TPV and differential charging measurements with C. M. W. and M. S. A. R. contributed to the analysis of PL data and development of the setup. L. K. fabricated SnO_2 based cells and films and performed corresponding electrical characterizations. F. Z. performed UPS measurements and interpreted corresponding data. S. A. developed SnO_2 based cells and films. N. K. performed UPS measurements and interpreted corresponding data. T. K. contributed to the analysis of recombination losses and analysed the simulation results. M. Sa. fabricated TiO_2 based cells and films and performed corresponding electrical characterizations. T. U. performed numerical simulations and analysed simulation results, contributed to the analysis of PL measurements and recombination losses. D. N. contributed to project planning, manuscript drafting and analysis of all electro-optical measurements. All co-authors contributed to proof reading of the manuscript.

Data availability

The data that support the plots within this paper and other findings of this study are available from the corresponding authors upon reasonable request.

Conflicts of interest

The authors declare no competing financial interests.

Acknowledgements

We thank Lukas Fiedler and Frank Jaiser for lab assistance. Florian Dornack and Andreas Pucher for providing measurement and laboratory equipment. Philipp Tockhorn for characterization of SnO_2 based cells. This work was in part funded by HyPerCells (a joint graduate school of the Potsdam University and the HZB) and by the Deutsche Forschungsgemeinschaft (DFG, German Research Foundation) – Project-ID 182087777 – SFB 951.

References

1 N. J. Jeon, H. Na, E. H. Jung, T.-Y. Yang, Y. G. Lee, G. Kim, H.-W. Shin, S. Il Seok, J. Lee and J. Seo, *Nat. Energy*, 2018, **3**, 682–689.
2 W. Tress, *Adv. Energy Mater.*, 2017, **7**, 1602358.
3 D. Bi, C. Yi, J. Luo, J.-D. Décoppet, F. Zhang, S. M. Zakeeruddin, X. Li, A. Hagfeldt and M. Grätzel, *Nat. Energy*, 2016, **1**, 16142.
4 T. S. Sherkar, C. Momblona, L. Gil-Escrig, J. Ávila, M. Sessolo, H. J. Bolink and L. J. A. Koster, *ACS Energy Lett.*, 2017, **2**, 1214–1222.
5 X. Zheng, B. Chen, J. Dai, Y. Fang, Y. Bai, Y. Lin, H. Wei, X. C. Zeng and J. Huang, *Nat. Energy*, 2017, **2**, 17102.
6 W. S. Yang, B. Park, E. H. Jung, N. J. Jeon, Y. C. Kim, D. U. Lee, S. S. Shin, J. Seo, E. K. Kim, J. H. Noh and S. Il Seok, *Science*, 2017, **356**, 1376–1379.
7 M. Saliba, T. Matsui, K. Domanski, J.-Y. Seo, A. Ummadisingu, S. M. Zakeeruddin, J.-P. J.-P. Correa-Baena, W. R. Tress, A. Abate, A. Hagfeldt, M. Grätzel and M. Gratzel, *Science*, 2016, **354**, 206.
8 M. Saliba, T. Matsui, J.-Y. Seo, K. Domanski, J.-P. Correa-Baena, M. K. Nazeeruddin, S. M. Zakeeruddin, W. Tress, A. Abate, A. Hagfeldt and M. Grätzel, *Energy Environ. Sci.*, 2016, **9**, 1989–1997.
9 M. Abdi-Jalebi, Z. Andaji-Garmaroudi, S. Cacovich, C. Stavrakas, B. Philippe, J. M. Richter, M. Alsari, E. P. Booker, E. M. Hutter, A. J. Pearson, S. Lilliu, T. J. Savenije, H. Rensmo, G. Divitini, C. Ducati, R. H. Friend and S. D. Stranks, *Nature*, 2018, **555**, 497–501.
10 X. Li, D. Bi, C. Yi, J.-D. Décoppet, J. Luo, S. M. Zakeeruddin, A. Hagfeldt and M. Grätzel, *Science*, 2016, **8060**, 1–10.
11 J.-P. Correa-Baena, W. Tress, K. Domanski, E. H. Anaraki, S.-H. Turren-Cruz, B. Roose, P. P. Boix, M. Grätzel, M. Saliba, A. Abate and A. Hagfeldt, *Energy Environ. Sci.*, 2017, **10**, 1207–1212.
12 K. Tvingstedt, L. Gil-Escrig, C. Momblona, P. Rieder, D. Kiermasch, M. Sessolo, A. Baumann, H. J. Bolink and V. Dyakonov, *ACS Energy Lett.*, 2017, **2**, 424–430.
13 C. M. Wolff, F. Zu, A. Paulke, L. P. Toro, N. Koch and D. Neher, *Adv. Mater.*, 2017, **29**, 1700159.
14 Y. Yang, M. Yang, D. T. Moore, Y. Yan, E. M. Miller, K. Zhu and M. C. Beard, *Nat. Energy*, 2017, **2**, 1–7.
15 E. M. Hutter, J. J. Hofman, M. L. Petrus, M. Moes, R. D. Abellón, P. Docampo and T. J. Savenije, *Adv. Energy Mater.*, 2017, **7**, 1–8.
16 E. Guillén, F. J. Ramos, J. A. Anta, S. Ahmad, E. Guille, F. J. Ramos, J. A. Anta and S. Ahmad, *J. Phys. Chem. C*, 2014, **118**, 22913–22922.
17 F. Staub, H. Hempel, J. C. Hebig, J. Mock, U. W. Paetzold, U. Rau, T. Unold and T. Kirchartz, *Phys. Rev. Appl.*, 2016, **6**, 1–13.
18 B. Krogmeier, F. Staub, D. Grabowski, U. Rau and T. Kirchartz, *Sustainable Energy Fuels*, 2018, **2**, 1027–1034.
19 D. Kiermasch, A. Baumann, M. Fischer, V. Dyakonov and K. Tvingstedt, *Energy Environ. Sci.*, 2018, **11**, 629–640.
20 M. Stolterfoht, C. M. Wolff, J. A. Márquez, S. Zhang, C. J. Hages, D. Rothhardt, S. Albrecht, P. L. Burn, P. Meredith, T. Unold and D. Neher, *Nat. Energy*, 2018, **3**, 847–854.
21 V. Sarritzu, N. Sestu, D. Marongiu, X. Chang, S. Masi, A. Rizzo, S. Colella, F. Quochi, M. Saba, A. Mura and G. Bongiovanni, *Sci. Rep.*, 2017, **7**, 44629.
22 I. L. Braly and H. W. Hillhouse, *J. Phys. Chem. C*, 2016, **120**, 893–902.
23 G. El-Hajje, C. Momblona, L. Gil-Escrig, J. Ávila, T. Guillemot, J.-F. Guillemoles, M. Sessolo, H. J. Bolink and L. Lombez, *Energy Environ. Sci.*, 2016, **131**, 6050–6051.
24 G. H. Bauer, L. Gütay and R. Kniese, *Thin Solid Films*, 2005, **480–481**, 259–263.
25 A. Delamarre, L. Lombez and J.-F. Guillemoles, *Appl. Phys. Lett.*, 2012, **100**, 131108.
26 P. Schulz, E. Edri, S. Kirmayer, G. Hodes, D. Cahen and A. Kahn, *Energy Environ. Sci.*, 2014, **7**, 1377.
27 L. E. Polander, P. Pahner, M. Schwarze, M. Saalfrank, C. Koerner and K. Leo, *APL Mater.*, 2014, **2**, 1–6.
28 I. Gelmetti, N. F. Montcada, A. Pérez-Rodríguez, E. Barrena, C. Ocal, I. García-Benito, A. Molina-Ontoria, N. Martín, A. Vidal-Ferran and E. Palomares, *Energy Environ. Sci.*, 2019, **12**, 1309–1316.
29 R. A. Belisle, P. Jain, R. Prasanna, T. Leijtens and M. D. McGehee, *ACS Energy Lett.*, 2016, **1**, 556–560.
30 Y. Hou, X. Du, S. Scheiner, D. P. McMeekin, Z. Wang, N. Li, M. S. Killian, H. Chen, M. Richter, I. Levchuk, N. Schrenker, E. Spiecker, T. Stubhan, N. A. Luechinger, A. Hirsch, P. Schmuki, H.-P. Steinrück, R. H. Fink, M. Halik, H. J. Snaith and C. J. Brabec, *Science*, 2017, **358**, 1192–1197.
31 W. S. Yang, J. H. Noh, N. J. Jeon, Y. C. Kim, S. Ryu, J. Seo and S. Il Seok, *Science*, 2015, **348**, 1234–1237.
32 M. Stolterfoht, C. M. Wolff, Y. Amir, A. Paulke, L. Perdigón-Toro, P. Caprioglio and D. Neher, *Energy Environ. Sci.*, 2017, **10**, 1530–1539.
33 X. Zheng, B. Chen, J. Dai, Y. Fang, Y. Bai, Y. Lin, H. Wei, X. C. C. Zeng and J. Huang, *Nat. Energy*, 2017, **2**, 17102.

34 Q. Wang, Q. Dong, T. Li, A. Gruverman and J. Huang, *Adv. Mater.*, 2016, **28**, 6734–6739.
35 C. C. Chueh, C. Z. Li and A. K. Y. Jen, *Energy Environ. Sci.*, 2015, **8**, 1160–1189.
36 H. Wei, Y. Fang, P. Mulligan, W. Chuirazzi, H.-H. Fang, C. Wang, B. R. Ecker, Y. Gao, M. A. Loi, L. Cao and J. Huang, *Nat. Photonics*, 2016, **10**, 333–339.
37 S. Zhang, M. Stolterfoht, A. Armin, Q. Lin, F. Zu, J. Sobus, H. Jin, N. Koch, P. Meredith, P. L. Burn and D. Neher, *ACS Appl. Mater. Interfaces*, 2018, **10**, 21681–21687.
38 L. Calió, S. Kazim, M. Grätzel and S. Ahmad, *Angew. Chem., Int. Ed.*, 2016, **55**, 14522–14545.
39 A. Gheno, S. Vedraine, B. Ratier and J. Bouclé, *Metals*, 2016, **6**, 21.
40 Y. Shao, Y. Yuan and J. Huang, *Nat. Energy*, 2016, **1**, 1–6.
41 P. Tiwana, P. Docampo, M. B. Johnston, H. J. Snaith and L. M. Herz, *ACS Nano*, 2011, **5**, 5158–5166.
42 W. Shockley and H. J. Queisser, *J. Appl. Phys.*, 1961, **32**, 510–519.
43 T. Kirchartz and U. Rau, *Phys. Status Solidi A*, 2008, **205**, 2737–2751.
44 U. Rau, D. Abou-Ras and T. Kirchartz, *Advanced Characterization Techniques for Thin Film Solar Cells*, Wiley, 2011.
45 P. Wurfel, *J. Phys. C: Solid State Phys.*, 1982, **15**, 3967–3985.
46 K. Tvingstedt and C. Deibel, *Adv. Energy Mater.*, 2016, **6**, 1502230.
47 W. Tress, N. Marinova, O. Inganäs, M. K. Nazeeruddin, S. M. Zakeeruddin and M. Grätzel, *Adv. Energy Mater.*, 2015, **5**, 1400812.
48 K. Tvingstedt, O. Malinkiewicz, A. Baumann, C. Deibel, H. J. Snaith, V. Dyakonov and H. J. Bolink, *Sci. Rep.*, 2014, **4**, 6071.
49 I. L. Braly, D. W. DeQuilettes, L. M. Pazos-Outón, S. Burke, M. E. Ziffer, D. S. Ginger and H. W. Hillhouse, *Nat. Photonics*, 2018, **12**, 355–361.
50 D. Luo, W. Yang, Z. Wang, A. Sadhanala, Q. Hu, R. Su, R. Shivanna, G. F. Trindade, J. F. Watts, Z. Xu, T. Liu, K. Chen, F. Ye, P. Wu, L. Zhao, J. Wu, Y. Tu, Y. Zhang, X. Yang, W. Zhang, R. H. Friend, Q. Gong, H. J. Snaith and R. Zhu, *Science*, 2018, **360**, 1442–1446.
51 Z. Liu, L. Krückemeier, B. Krogmeier, B. Klingebiel, J. A. Márquez, S. Levcenko, S. Öz, S. Mathur, U. Rau, T. Unold and T. Kirchartz, *ACS Energy Lett.*, 2019, **4**, 110–117.
52 P. Caprioglio, F. Zu, C. M. Wolff, J. A. Márquez Prieto, M. Stolterfoht, P. Becker, N. Koch, T. Unold, B. Rech, S. Albrecht and D. Neher, *Sustainable Energy Fuels*, 2019, **3**, 550–563.
53 J. Wang, W. Fu, S. Jariwala, I. Sinha, A. K. Y. Jen and D. S. Ginger, *ACS Energy Lett.*, 2019, **4**, 222–227.
54 M. Burgelman, P. Nollet and S. Degrave, *Thin Solid Films*, 2000, **362**, 527–532.
55 P. Calado, A. M. Telford, D. Bryant, X. Li, J. Nelson, B. C. O'Regan and P. R. F. Barnes, *Nat. Commun.*, 2016, **7**, 1–10.
56 F. Zu, C. M. Wolff, M. Ralaiarisoa, P. Amsalem, D. Neher and N. Koch, *ACS Appl. Mater. Interfaces*, 2019, **11**, 21578–21583.
57 D. Kiermasch, L. Gil-Escrig, A. Baumann, H. J. Bolink, V. Dyakonov and K. Tvingstedt, *J. Mater. Chem. A*, 2019, **7**, 14712–14722.
58 S. G. M. Wheeler, PhD thesis, Bulk and Surface Recombination Limitations to High Voltage Solution Processed Solar Cells, Imperial College London, 2017, https://spiral.imperial.ac.uk/handle/10044/1/67751.
59 J. Hwang, F. Amy and A. Kahn, *Org. Electron.*, 2006, **7**, 387–396.
60 L. Kegelmann, P. Tockhorn, C. M. Wolff, J. A. Márquez, S. Caicedo-Dávila, L. Korte, T. Unold, W. Lövenich, D. Neher, B. Rech and S. Albrecht, *ACS Appl. Mater. Interfaces*, 2019, **11**, 9172–9181.
61 S. Pisoni, M. Stolterfoht, J. Löckinger, T. Moser, Y. Jiang, P. Caprioglio, D. Neher, S. Buecheler and A. N. Tiwari, *Sci. Technol. Adv. Mater.*, 2019, **20**, 786–795.
62 F. Sahli, J. Werner, B. A. Kamino, M. Bräuninger, R. Monnard, B. Paviet-Salomon, L. Barraud, L. Ding, J. J. Diaz Leon, D. Sacchetto, G. Cattaneo, M. Despeisse, M. Boccard, S. Nicolay, Q. Jeangros, B. Niesen and C. Ballif, *Nat. Mater.*, 2018, **17**, 820–826.
63 S. Zhang, S. M. Hosseini, R. Gunder, A. Petsiuk, P. Caprioglio, C. M. Wolff, S. Shoaee, P. Meredith, S. Schorr, T. Unold, P. L. Burn, D. Neher and M. Stolterfoht, *Adv. Mater.*, 2019, 1901090.
64 H. Tsai, W. Nie, J. C. Blancon, C. C. Stoumpos, R. Asadpour, B. Harutyunyan, A. J. Neukirch, R. Verduzco, J. J. Crochet, S. Tretiak, L. Pedesseau, J. Even, M. A. Alam, G. Gupta, J. Lou, P. M. Ajayan, M. J. Bedzyk, M. G. Kanatzidis and A. D. Mohite, *Nature*, 2016, **536**, 312–317.